CARTA: Coordinated Arrangement of Receivers for Target Acquisition

Alireza Famili*, Angelos Stavrou*†
*WayWave Inc, Virginia, USA
†Department of Electrical & Computer Engineering, Virginia Tech, Virginia, USA
afamili@waywave.com, angelos@vt.edu

***Abstract*—The growing necessity for monitoring and identification of unmanned aerial systems (UASs) in restricted zones is paramount. Current strategies are inadequate for effectively tracking stealthy UASs, posing significant risks to both military and civilian domains. Although radar is renowned for its detection strength, its conventional active systems, where transmitters and receivers are co-located, encounter numerous challenges. A promising alternative is a passive radar, utilizing existing ambient signals, thus eliminating the need for a dedicated transmitter. In this context, we propose *CARTA*, a novel approach that utilizes spaceborne illuminators, particularly suited for tasks requiring extensive operational reach, such as high-altitude surveillance of missiles and fighter jets. Despite the chosen emitter type, challenges in range measurement and target localization persist, primarily due to the unknown position of transmitters. *CARTA* addresses this issue by adopting time difference of arrival (TDOA) techniques coupled with bistatic Doppler shift analysis. A critical, yet overlooked factor in passive radar systems is the impact of the geometric arrangement of receivers on localization accuracy. *CARTA* emphasizes the importance of optimizing receiver placement to minimize geometry-induced errors, recognizing the complexity of this NP-hard optimization problem. Our results indicate that *CARTA* significantly enhances localization accuracy compared to systems with arbitrary deployments.**

***Index Terms*—passive radars, spaceborne illumination, localization, TDOA, Doppler shift, GDOP, optimal placement**

I. Introduction

As of August 2021, the Federal Aviation Administration (FAA) documented more than 100 monthly close encounters between aircraft and unmanned aerial systems (UASs) [1], underscoring an urgent requirement for reliable detection and monitoring of UASs in off-limits airspace. Present strategies are insufficient for the early detection and tracking of low-observable stealthy UASs, presenting serious safety hazards across different areas such as defense and civilian sectors.

Radar technology, noted for its effective detection and sensing abilities, typically uses active monostatic setups where transmitters and receivers are situated together. Yet, these configurations are constrained by their expensive nature, significant energy requirements, reliance on a single viewpoint for observation, and requirement for transmission permits [2].

Passive radar presents a practical alternative, leveraging existing radio frequency (RF) signals and eliminating the necessity for a dedicated transmitter, which leads to lower running costs and less visibility, thereby improving stealth capabilities [3]. It can be set up in bistatic or multistatic modes, enhancing spatial coverage and resolution [4]. However, it encounters difficulties in accurately pinpointing target distance and position because it depends on external RF sources that cannot be controlled.

ISBN 978-3-903176-63-8 © 2024 IFIP

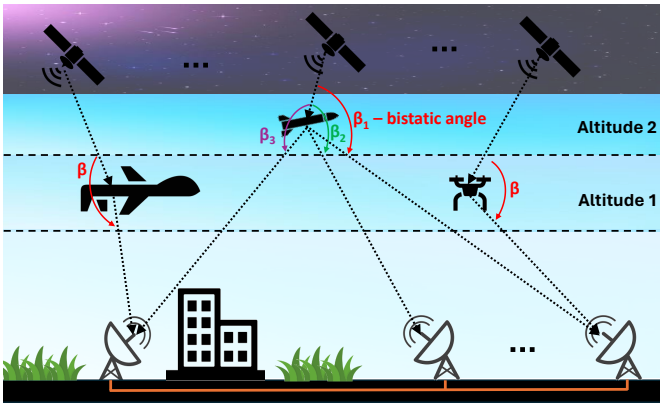

Figure 1: Overview of detection and localization of intruder objects in passive radar setup with spaceborne IOO

In passive radar technology, selecting emitters is crucial for defining the system's functionalities and potential uses. Various sources, from ground-based ones like Wireless Fidelity (Wi-Fi) signals for indoor settings to 5G cell towers for outdoor areas, provide a range of options. Yet, for a wider operational reach, especially in high-altitude aerial surveillance for tracking entities like missiles and fighter jets, space-based sources stand out as more effective. Low Earth Orbit (LEO) satellites, particularly with the expanding installation of networks such as Starlink, are seen as highly advantageous due to their comprehensive coverage and low-latency features.

In this paper, we propose ***CARTA: Coordinated Arrangement of Receivers for Target Acquisition***. Despite *CARTA* being fully adaptable to any type of emitter, whether terrestrial, airborne, or spaceborne, we utilize LEO satellites with a special focus on Starlink constellation as a prime example to demonstrate our methodology, given their promising potential. We explore methodologies for utilizing these satellites as emitters, examining both backscatter and forwardscatter approaches. While backscatter, which involves the reflection of signals from the target back to the receiver, is a popular method, forwardscatter offers enhanced Radar Cross Section (RCS) for detecting low-observable objects. However,

the presumption of constant accessibility to forwardscatter scenarios might not be viable, necessitating a fallback on backscatter techniques under certain conditions. Figure 1 represents a visual summary of *CARTA*.

Crucially, irrespective of the scattering technique employed, the challenge of range measurement and target localization persists due to the unknown positioning of the LEO satellite transmitters. To mitigate this, *CARTA* advocates for time difference of arrival (TDOA) methods, leveraging the temporal discrepancy in signal reception across a network of surveillance receivers relative to a reference receiver. This approach effectively nullifies the uncertainty associated with the transmitter's position. Complementing this, Doppler shift analysis facilitates the determination of the target's velocity and trajectory.

Our findings demonstrate that both the ranging and geometry-induced errors influence the total positioning accuracy of a TDOA-based passive radar system. For example, in situations where the ranging error is kept under 1 m, the geometric dilution of precision (GDOP) at a certain spot is calculated to be 20. This leads to an eventual localization inaccuracy of approximately 20 meters (calculated as $1\ m\ \times\ 20\ =\ 20\ m$). This increase in error from 1 m to 20 m is deemed inappropriate for high-accuracy target positioning applications.

Our main goal is to examine the effects of GDOP and to refine the arrangement of receivers, an important factor that has been neglected in passive radar systems. While existing studies [5]–[8] have focused mainly on reducing ranging errors to improve positioning precision, *CARTA* addresses aspects associated with the spatial geometric setup of the system.

Utilizing a novel optimization framework based on the evolutionary algorithm (EA) category, we tackle the NP-Hard challenge of identifying the optimal locations for receiver placement, thus attaining high accuracy in target positioning. In support of this effort, we calculate the positioning error bound (PEB) for *CARTA*, highlighting that the error in localization using TDOA-based trilateration methods stems from both inaccuracies in range measurement and the geometric relationship between the target and the positioning nodes (receivers).

Our experimental verifications show that even when ranging errors are minimal, a poor GDOP can greatly reduce the accuracy of target localization in a three-dimensional (3D) environment. By using coverage heatmaps, we demonstrate that GDOP results from both vertical and horizontal dilution of precision (VDOP and HDOP), with vertical dilution having a more significant impact on lowering the accuracy of estimates than horizontal. This underscores the effectiveness of *CARTA* for identifying the best receiver placement to accurately determine the target's location, affecting both the horizontal ($X-Y$ plane) and vertical (Z-axis) dimensions.

The summary of our contributions is detailed below.

- We introduce *CARTA*, a passive radar detection system capable of determining the position, speed, and heading of UASs in 3D space, with unknown emitter locations.
- As a prime example, *CARTA* utilizes Starlink satellites for illumination, capitalizing on the advantageous features of the LEO constellation to ensure broad coverage and high-resolution capabilities necessary for detecting low-observable UASs.
- *CARTA* demonstrates, through the derivation of the PEB for a TDOA-based localization system, that the total error is influenced by two factors: errors stemming from ranging measurements and errors caused by the spatial geometric relationship between the receivers and the target.
- *CARTA* introduces a new optimization algorithm, rooted in the EA class, designed to address the NP-Hard issue of determining the optimal placement of receivers to minimize errors caused by geometric factors.
- Through conducting an extensive simulation campaign that mirrors real-world conditions, we assess the efficacy of *CARTA*. Our findings indicate that *CARTA* achieves an improvement in the accuracy of location estimation that is over tenfold greater than that of other configurations lacking optimal receiver placement.

II. Related Work

Spaceborne IOO: The body of research on using multistatic radar to detect aerial systems with spaceborne illuminators of opportunity (IOO) is expanding [9]–[11]. This research primarily focuses on the utilization of current Medium Earth Orbit (MEO) [12] and geostationary (or geosynchronous equatorial orbit, known as GEO) [13] satellite constellations. However, these do not offer adequate spatial coverage and depend on the presence of one or more transmitters, which poses a problem for radar systems needing operational flexibility across different areas. For instance, numerous digital television satellites are positioned in geostationary orbits, tailored to cover densely populated regions. Consequently, they fail to provide coverage over oceans and vast areas of less developed territories.

Antoniou et al. [13] harnessed transmissions from global navigation satellite systems (GNSS) for imaging purposes within a passive bistatic backscattering arrangement, highlighting the significance of utilizing expansive MEO satellite constellations. They contended that the value of radar imagery is heightened when multiple images, collected over time, are available to examine changes in the environment. In another instance, Gronowski et al. [14] employed transmissions from the Global Navigation Satellite System (GPS) for the passive bistatic detection of an airborne Boeing 737-45D, utilizing the forward scattering signal. Utilizing Digital Video Broadcasting (DVB) transmissions offers the advantage of high transmission power, yet these signals fail to cover many areas. GPS signals are analyzed using affordable Universal Software Radio Peripheral (USRP) N210 software-defined radios (SDR) equipped with adaptable RF front ends. Burov et al. [15] conducted passive bistatic detection of a Boeing 737-524, utilizing the forward scattered signal from an Intelsat GEO

transmitter. Abdullah et al. [16] carried out passive bistatic detection of a DJI Phantom quadcopter by leveraging the forward scattered signal from a DVB satellite at 11.725 GHz. They were able to detect micro-Doppler effects within the received signal, which were attributed to the movement of the quadcopter's blades.

McDowell [9] highlights the recent surge in the deployment of LEO constellations, such as SpaceX's Starlink, which offer extensive global coverage and operate at higher frequencies to improve object detection capabilities around the world. This development allows operators to set up multiple, affordable receivers in diverse locations, facilitating the real-time, covert detection and tracking of objects.

Optimal Deployment of Receivers: In recent times, significant research efforts have been devoted to optimizing the placement of anchors, with studies targeting both indoor localization [17]–[21] and the configuration of wireless networks [22], [23]. These studies mainly aim to ascertain the optimal number of anchors required to adequately cover a specific indoor area, a factor largely dependent on the type of sensor technology utilized. Nonetheless, the challenge of optimally deploying a predetermined number of sensors to minimize errors linked to the spatial relationship between the localization sensors and the target has yet to be thoroughly explored. To this end, our proposed system primarily focuses on enhancing localization accuracy through the strategic placement of receivers within a passive radar framework. To our knowledge, we are the pioneers in identifying and addressing this challenge in the realm of passive radar localization.

III. Target Detection Framework

In this section, we begin by offering a concise overview of spaceborne illuminators and various radar configurations in Section III-A. Subsequently, in Section III-B, we introduce the framework utilized by *CARTA* for localizing the target and determining its velocity and heading.

A. Passive Radar Spaceborne Illumination

Passive radar systems rely on existing transmissions from non-cooperative sources, meaning they do not generate their own signals. Instead, they depend on capturing ambient signals reflected off objects, which originate from unintended IOO, contrasting with traditional radar systems that emit their own signals for detection and tracking purposes [24].

Spaceborne illuminators are particularly valued in passive radar systems for their wide coverage, steady signal presence, and high vantage point. Their global coverage, along with the capability to illuminate areas lacking terrestrial signals, greatly improves the detection capabilities and operational versatility of passive radar setups. In spaceborne passive radar applications, selecting between LEO, MEO, and GEO satellites hinges on the application's specific needs. Nonetheless, for many applications, LEO satellites are often preferred due to their lower latency, reduced signal loss, and enhanced resolution capabilities. Table I provides an in-depth comparison of the various satellite constellations, detailing their operational frequency ranges, altitudes, and the number of satellites in each constellation. Additionally, their relative working altitudes are visually depicted for comparison in Figure 2a, offering a clear overview of the differences in their orbital positions.

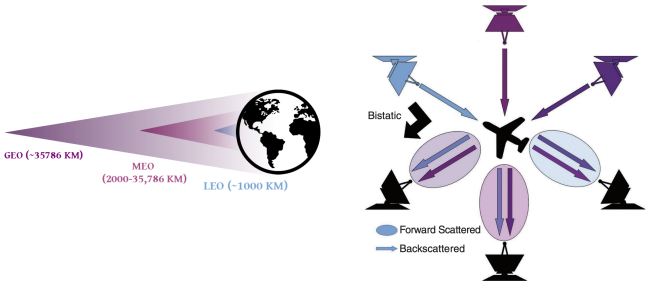

(a) (b)

Figure 2: (a) GEO, MEO, and LEO orbitals; (b) Representation of backscatter vs. forwardscatter radar configurations

Table I: Comprehensive Overview of Spaceborne Illuminators

Low Earth Orbit			
Constellation	Frequency (MHz)	Altitude (km)	Population
Globalstar	2484	1414	48
Iridium	1621	780	75
Starlink	Ku, Ka, V	550, 1110, 340	>1600
Medium Earth Orbit			
Constellation	Frequency (MHz)	Altitude (km)	Population
GPS	1575, 1227, 1176	20200	24
GLONASS	1602, 1246	19100	24
Galileo	1575	20505	24
BeiDou	1561, 1207, 1268	21528	24
Geostationary/Geosynchronous Orbit			
Constellation	Frequency (MHz)	Altitude (km)	Population
NAVIC	1176, 2492	35786	7
Inmarsat	1626	35405	13

Figure 2b provides a graphical illustration of various radar setups. Backscatter radar functions by capturing signals bounced back from a target, where the bistatic range is the cumulative distance the signal traverses from the transmitter to the target and subsequently to the receiver, as illustrated in Figure 3a. When the bistatic angle; the angle spanning from the transmitter to the target and then to the receiver, nears 180°, the system shifts to a forwardscatter mode. In this configuration, the radar identifies disturbances in the signal's path caused by the target's direct interference with the line connecting the transmitter and receiver. This mode is particularly effective for detecting low-observable entities due to the unique pattern of signal distortion it creates.

Contemporary aerial systems frequently attain low radar visibility through either small dimensions or sophisticated countermeasures such as radar-absorbing material (RAM) coatings. These features mainly contribute to reduced observability in terms of the target's backscatter Radar RCS. However, this principle does not apply in forwardscatter con-

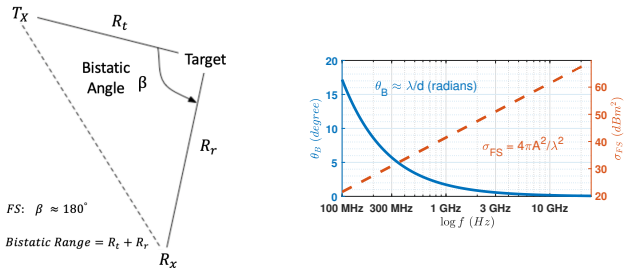

(a) (b)

Figure 3: (a) Forwardscatter RCS (σ_{FS}) and angular width of scatter (θ_B) for an idealised medium-sized air-born target with the $A = 10\ m^2$ and $d = 10\ m$; (b) Bistatic range and angle

figurations, wherein a passive receiver detects the shadowing effect produced when a target crosses the direct path between a transmitter and the receiver. In a forwardscatter situation, the RCS for an RF opaque target is calculated as

$$\sigma_{FS} = \frac{4\pi A^2}{\lambda^2}; \tag{1}$$

where A represents the silhouette area of the target, and λ denotes the wavelength of the signal emitted by the transmitter. Significantly large RCS values arise when the wavelength of the transmitted signal is small compared to the target's size.

As depicted in Figure 3b, an increase in frequency leads to a higher forwardscatter RCS but results in a narrower angular width of the forwardscatter signal. In a single bistatic radar system, this reduced angular width translates to a shorter duration of observation at the receiver, adversely affecting detection capability. The analysis presented in [11] suggests that the ultra-high frequency (UHF) range is the most suitable for forwardscatter radar detection using a single bistatic pair. However, we argue that in extensive multistatic radar networks, the issue of reduced angular width at higher frequencies is less significant. At the Ka-band frequency (27GHz to 40 GHz), the forwardscatter RCS of a target is significantly amplified, surpassing the RCS levels achievable at UHF frequencies.

B. Localization, Speed, and Heading

Passive radar's capability to localize and determine the speed and heading of a target, even without knowing the emitter's location, relies on signal processing techniques and geometrical considerations. *CARTA* employs the bistatic range and bistatic range rate to achieve these goals. Let R_t be the distance from the transmitter to the target, and R_r be the distance from the receiver to the target, then the bistatic range is as

$$R_{bistatic} = R_t + R_r. \tag{2}$$

Given that the position of the emitter is not known, *CARTA* employs TDOA-based triangulation techniques, utilizing multiple passive receivers to pinpoint the target's location. In a setup involving a single target and N receivers, the signal from the emitter bounces off the target and is captured by the N receivers. If Δt_{ij} denotes the TDOA for the signal reflection from the target between receiver i and receiver j, and c represents the speed of light, the difference in distance to the target from the two receivers is expressed as

$$(R_t + R_{r,i}) - (R_t + R_{r,j}) = R_{r,i} - R_{r,j} = c \cdot \Delta t_{ij}; \tag{3}$$

where $R_{r,i}$ and $R_{r,j}$ are the distances between the target to receiver i and receiver j, respectively. By combining the TDOA measurements from multiple pairs of receivers, *CARTA* estimates the target's position using hyperbolic multilateration techniques. In other words, the TDOA measurements correspond to the differences in distances from the target to the receivers, leading to a set of hyperbolic equations. For each pair of receivers (i, j), the locus of possible target positions that satisfy the TDOA measurement Δt_{ij} is a hyperbola, with the foci at the positions of the two receivers. The target lies on one of the branches of this hyperbola. The equation of the hyperbola derived from the TDOA between receivers i and j can be expressed as

$$c \cdot \Delta t_{ij} = \sqrt{(x - x_i)^2 + (y - y_i)^2 + (z - z_i)^2} - \sqrt{(x - x_j)^2 + (y - y_j)^2 + (z - z_j)^2}; \tag{4}$$

where (x_i, y_i, z_i) and (x_j, y_j, z_j) are the known positions of receivers i and j, and (x, y, z) is the unknown position of the target. In practice, more than two receivers are used to improve the accuracy and resolve the ambiguity in target positioning. Each pair of receivers provides a hyperbolic equation, and the target's position is estimated at the intersection of these hyperbolas. With N receivers, we can form $N(N-1)/2$ pairs, each providing a TDOA measurement and a corresponding hyperbolic equation.

Typically, to localize a target in a two-dimensional (2D) space using trilateration, at least three anchor nodes are required. When this concept is expanded to three dimensions, the necessity increases to a minimum of four sources. Resolving the collection of hyperbolic equations together yields the target's coordinates, which can be articulated as

$$[x\ y\ z]^T = \min \quad e(x, y, z); \tag{5}$$

where $[x\ y\ z]^T$ is the location of the target in a Cartesian coordinate system and $e(x, y, z)$ is defined as:

$$e(x, y, z) = \sum_{i=1}^{N-1} \left\{ (r_i - r_j) - \sqrt{(x_i - x_j)^2 + (y_i - y_j)^2 + (z_i - z_j)^2} \right\};$$

where $[x_i\ y_i\ z_i]^T$ values are the Cartesian coordinates of the $i-$th receiver. In practice, owing to the measurement noise and inaccuracies, the hyperbolas may not intersect at a single point. Various algorithms, such as the Least Squares method, can be employed to find the best estimate of the target's position that minimizes the total error.

In passive radar systems, especially when the location of the emitter is unknown, estimating the target's speed and

heading involves analyzing the bistatic Doppler shifts observed at multiple receivers. These receivers detect signals from non-cooperative transmitters (emitters) reflected off moving targets. The Doppler shift provides information about the relative velocity of the target with respect to both the transmitter and the receiver.

In a bistatic radar configuration, where the transmitter (emitter) and receiver are spatially separated, the bistatic Doppler shift (f_d) at the receiver can be expressed as

$$f_d = \frac{f_c}{c}(\vec{v}_t \cdot \hat{r}_t - \vec{v}_r \cdot \hat{r}_r); \tag{6}$$

where f_c is the carrier frequency of the transmitted signal; c is the speed of light; $\vec{v}_t$ is the velocity vector of the target; $\vec{v}_r$ is the velocity vector of the receiver (often zero if the receiver is stationary); $\hat{r}_t$ is the unit vector from the target to the transmitter; $\hat{r}_r$ is the unit vector from the target to the receiver. The terms $\vec{v}_t \cdot \hat{r}_t$ and $\vec{v}_r \cdot \hat{r}_r$ represent the radial velocities of the target relative to the transmitter and receiver, respectively.

Similar to the localization framework, *CARTA* employs multiple receivers to estimate the target's velocity vector and heading. Each receiver provides a bistatic Doppler shift measurement, and by combining these measurements, the motion of the target is calculated. Assume we have N receivers, each detecting the bistatic Doppler shift, f_{d_i}, from the target. The velocity of the target, $\vec{v}_t$, influences the Doppler shifts observed at the receivers. By solving a system of equations based on the observed Doppler shifts and the known positions of the receivers, the velocity vector of the target is estimated.

Once the velocity vector of the target, $\vec{v}_t = (v_{tx}, v_{ty}, v_{tz})$, is estimated, the heading of the target, which is the angle in the horizontal plane between a reference direction (e.g., true north) and the projection of the velocity vector on that plane, can be determined. If the velocity vector in the horizontal plane is $\vec{v}_t = (v_{tx}, v_{ty})$, the heading θ can be calculated as $\theta = \arctan 2(v_{ty}, v_{tx})$. Lastly, the speed of the target is the magnitude of the velocity vector and can be computed as $v = \sqrt{v_{tx}^2 + v_{ty}^2 + v_{tz}^2}$.

IV. *CARTA* Localization Error Bounds & Optimal Receiver Placement

In this section, we begin by deriving the positioning error bound (PEB) on *CARTA* in Section IV-A, demonstrating that the overall localization accuracy is influenced by the spatial configuration of receivers relative to the target's location. Subsequently, in Section IV-B, we introduce the *CARTA* optimization framework aimed at addressing the NP-hard problem of optimal receiver deployment.

A. Localization Error Bounds

The Cramer Rao Lower Bound (CRLB) serves as a valuable measure for assessing the accuracy of localization by indicating the lowest possible variance in location that can be achieved when employing an unbiased estimator for positioning. By considering the conditions of independence and the presence of zero-mean Gaussian noise with a steady variance σ_r^2 in range determinations [17], we calculate the PEB for the passive radar setup.

As highlighted earlier, accurately determining r_i (where $r_i = R_{r,i}$) is impractical. However, it is possible to precisely calculate the difference $r_i - r_j$. Moving forward with the subsequent steps, we select r_0 to serve as the reference receiver and proceed to calculate the differences $r_i - r_0$ as follows

$$\begin{aligned} r_i - r_0 = &\sqrt{(x - x_i)^2 + (y - y_i)^2 + (z - z_i)^2} \\ &- \sqrt{(x - x_0)^2 + (y - y_0)^2 + (z - z_0)^2}. \end{aligned} \tag{7}$$

Given the inaccuracies in the ranging measurements, the exact value of $r_i - r_0$ cannot be determined, which introduces errors in determining $[x\ y\ z]^T$ as per Equation (7). To link the overall 3D positioning error, represented by $\sigma_T(x, y, z)$, with the errors in distance estimation, σ_{r_i}, arising from the process of signal measurement, it's critical to identify the variance of the 3D location estimator,

$$\sigma_T(x, y, z) = \sqrt{\sigma_x^2 + \sigma_y^2 + \sigma_z^2}; \tag{8}$$

where $(\sigma_x^2, \sigma_y^2, \sigma_z^2)$ represent the variances in error for the estimations along the $x-$, $y-$, and $z-$axis, respectively. Let $\mathbf{\Delta X} = [\Delta x\ \Delta y\ \Delta z]^T$ denote the derivative with respect to the estimations of $[x\ y\ z]^T$. Hence, for the variance in positioning, as per Equation (8), we have

$$\sigma_T^2(x, y, z) = \mathbf{Trace}\left(\mathbf{E}\left(\mathbf{\Delta X \Delta X^T}\right)\right); \tag{9}$$

and $\mathbf{Trace}(.)$ signifies the summation of the diagonal elements within a matrix. Following this, we explore the relationship between $\sigma_T^2(x, y, z)$ and the $\sigma_{r_i}^2$. This involves differentiating Equation (7), that is

$$\begin{aligned} \Delta r_i - \Delta r_0 = &\frac{\Delta x(x - x_i) + \Delta y(y - y_i) + \Delta z(z - z_i)}{\sqrt{(x - x_i)^2 + (y - y_i)^2 + (z - z_i)^2}} \\ &- \frac{\Delta x(x - x_0) + \Delta y(y - y_0) + \Delta z(z - z_0)}{\sqrt{(x - x_0)^2 + (y - y_0)^2 + (z - z_0)^2}}; \end{aligned} \tag{10}$$

where we omitted second- and higher-order terms for simplicity. In a localization system employing N passive receivers, Equation (10) is represented as $\mathbf{\Delta R_i - \Delta R_0 = \Psi \Delta X}$, or in another form, $\mathbf{\Delta X} = (\mathbf{\Psi}^T\mathbf{\Psi})^{-1}\mathbf{\Psi}^T(\mathbf{\Delta R_i - \Delta R_0})$; with $\mathbf{\Delta R_i} = [\Delta r_1\ \cdots\ \Delta r_{N-1}]^T$, $\mathbf{\Delta R_0} = [\mathbf{\Delta r_0}\ \cdots\ \mathbf{\Delta r_0}]^\mathbf{T}$, and

$$\mathbf{\Psi} = \begin{bmatrix} \frac{x-x_1}{r_1} - \frac{x-x_0}{r_0} & \frac{y-y_1}{r_1} - \frac{y-y_0}{r_0} & \frac{z-z_1}{r_1} - \frac{z-z_0}{r_0} \\ \vdots & \vdots & \vdots \\ \frac{x-x_{N-1}}{r_{N-1}} - \frac{x-x_0}{r_0} & \frac{y-y_{N-1}}{r_{N-1}} - \frac{y-y_0}{r_0} & \frac{z-z_{N-1}}{r_{N-1}} - \frac{z-z_0}{r_0} \end{bmatrix}.$$

It is reasonable to assume, for the sake of simplicity and without sacrificing generality, that the variance of r_i, Var(r_i), is equal to σ_r^2, and that the errors Δr_i are uncorrelated; Therefore

$$\mathbf{Cov}(\mathbf{\Delta X}) = \mathbf{\Phi}\left(\mathbb{I}_{\mathbf{N-1}} + \mathbb{J}_{\mathbf{N-1}}\right)\mathbf{\Phi}^T\sigma_r^2; \tag{11}$$

where $\mathbf{\Phi} = (\mathbf{\Psi}^T\mathbf{\Psi})^{-1}\mathbf{\Psi}^T$, $\mathbb{I}_{\mathbf{N-1}}$ is the identity matrix of size $(N-1)\times(N-1)$ and $\mathbb{J}_{\mathbf{N-1}}$ is the $(N-1)\times(N-1)$ matrix with

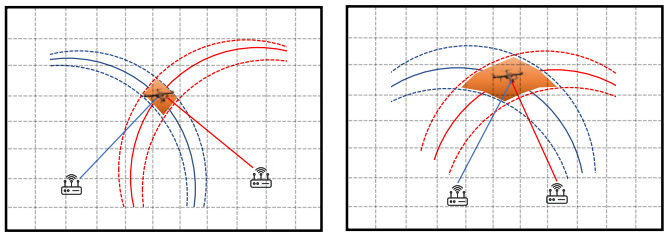

(a) Receiver anchor placement with low localization error

(b) Receiver anchor placement with high localization error

Figure 4: Comparison of GDOP on location estimation error due to different anchor placement

Table II: Evaluation of GDOP Values

GDOP Values	Evaluation of the Geometry
1	Ideal
$1-2$	Very Good
$2-5$	Good
$5-10$	Medium
$10-20$	Sufficient
>20	Bad

all its entries equal to one. Drawing from Equation (9), the variance associated with the 3D location estimator is detailed as follows

$$\sigma_T^2(x,y,z) = G(x,y,z)\cdot\sigma_r^2; \tag{12}$$

and $G(x,y,z)$ is expressed as follows

$$G(x,y,z) = \mathbf{Trace}\left(\mathbf{\Phi}(\mathbb{I}_{\mathbf{N-1}} + \mathbb{J}_{\mathbf{N-1}})\mathbf{\Phi}^T\right). \tag{13}$$

Consequently, the total accuracy of the location determination is impacted by the geometry-induced error $G(x,y,z)$, which is exclusively governed by the spatial arrangement between the localization receiver anchors and the target. In satellite navigation, $G(x,y,z)$ is referred to as Geometric Dilution of Precision (GDOP), a concept that describes how the arrangement of navigation satellites influences the accuracy of positional measurements through error propagation in a mathematical context. GDOP is composed of Horizontal Dilution of Precision (HDOP) and Vertical Dilution of Precision (VDOP), where $GDOP = \sqrt{HDOP^2 + VDOP^2}$. HDOP, denoted as $G(x,y)$, illustrates the influence of the spatial relationship between the receivers and the target in the $X-Y$ plane. Meanwhile, VDOP, represented as $G(z)$, indicates the effect of spatial arrangement on the estimation along the Z-axis. Table II shows the evaluation of the GDOP values.

The visual depiction of GDOP is showcased in Figure 4 across two different settings. In the initial scenario, depicted in Figure 4a, the positioning of the localization anchors (passive radar receivers) is more advantageous than the arrangement presented in Figure 4b. This difference in configuration results in distinct errors in location estimation, as highlighted by the shaded areas in each figure.

Our goal is to achieve an optimal GDOP while maintaining low HDOP and VDOP values at the same time. A scenario with a favorable HDOP but unfavorable VDOP leads to precise 2D localizations with imprecise estimations along the Z-axis. This means while the target's position on the $X-Y$ plane is accurately estimated within the area, there could be significant errors in determining the target's altitude. The majority of the existing research is centered around 2D localization [17], [21], often neglecting the importance of optimal anchor placement. However, for applications involving 3D environments, such as missile target localization and tracking, accurate estimations on the Z-axis are essential.

B. CARTA Deployment Strategies

Former approaches to localization mainly concentrated on fixed targets in 2D settings, thereby overlooking the complex spatial interrelations in three dimensions among the target and anchor points. This oversight has made the task of identifying the most advantageous positions for a moving target within a 3D environment a persisting challenge [21]. Moreover, the effort to configure anchor placements to minimize the relative geometric error between the passive radar system's receivers and the target in any location has been acknowledged as a recognized NP-Hard problem [17]–[19], [21].

In this work, we present an optimization algorithm specifically developed to identify the most favorable positioning of receivers to minimize the localization error caused by suboptimal spatial configurations. This algorithm is engineered to guarantee high accuracy in localization estimations, addressing both the horizontal ($X-Y$ plane) and vertical (Z-axis) dimensions.

The Z-axis is particularly prone to errors due to geometric considerations. A favorable overall GDOP at a specific point does not necessarily ensure that the VDOP will be equally advantageous compared to the HDOP at that same point. This discrepancy frequently results in accurate estimations on the $X-Y$ plane while leading to significant errors in the estimations along the Z-axis. To the best of our knowledge, we are the first to propose an algorithm aimed at enhancing the target localization accuracy in passive radar systems, encompassing both the $X-Y$ plane and the Z-axis.

In addressing the NP-Hard problem, we apply two constraints centered on the average values of $G(x,y)$ and $G(z)$. Once these averages align with our constraints, the configuration that yields the minimum $G(x,y,z)$ is deemed the optimal solution. While there may exist other configurations with comparable or lower $G(x,y,z)$ values, our main goal is to minimize the influence of anchor placement on the accuracy of location estimations for any potential target location. Thus, identifying a setup that adheres to our predefined averages for $G(x,y)$ and $G(z)$ achieves our objective. This strategy simplifies the optimization process, maintaining our dedication to reducing the effects of geometric discrepancies.

1) Problem Formulation: We aim to pinpoint the optimal deployment for a collection of five receivers by lowering the mean value of $G(x,y,z)$ over all points in the specified defense zone, represented as $\overline{G(x,y,z)}$, and ensuring that the mean values of $G(x,y)$ and $G(z)$, indicated as $\overline{G(x,y)}$ and $\overline{G(z)}$ respectively, do not exceed predetermined threshold

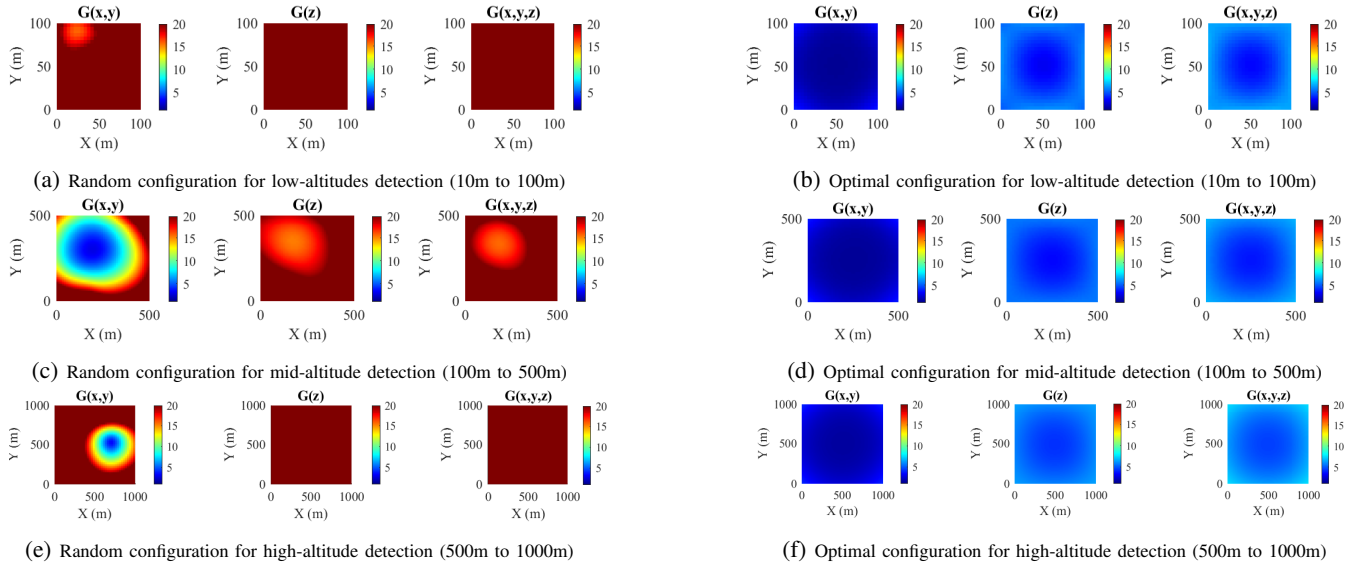

(a) Random configuration for low-altitudes detection (10m to 100m)

(b) Optimal configuration for low-altitude detection (10m to 100m)

(c) Random configuration for mid-altitude detection (100m to 500m)

(d) Optimal configuration for mid-altitude detection (100m to 500m)

(e) Random configuration for high-altitude detection (500m to 1000m)

(f) Optimal configuration for high-altitude detection (500m to 1000m)

Figure 5: Comparison of $G(.)$ Values: Random vs. Optimal Placement in Varied Altitudes

values. The final optimization formulation can be described as follows

$$\begin{aligned} \min \quad & \textstyle\sum_{\mathbb{T}} \mathbf{Trace}\left(\mathbf{\Phi}(\mathbb{I}_{\mathbf{N-1}} + \mathbb{J}_{\mathbf{N-1}})\mathbf{\Phi}^T\right) \\ s.t. \quad & \overline{G(x,y)} < h_T;\ \overline{G(z)} < v_T; \end{aligned}$$

where $\mathbb{T}$ represents the target domain, a subset of the environment encompassing every potential position for the target, $\mathbf{\Phi}$ is derived from Equation (12), and h_T and v_T stand for the threshold values for $\overline{G(x,y)}$ and $\overline{G(z)}$, correspondingly.

We aim to reduce $\overline{G(x,y,z)}$ to improve localization precision while imposing restrictions on $\overline{G(x,y)}$ and $\overline{G(z)}$ to ensure minimal errors in both horizontal and vertical estimations. This method ensures that enhancements in overall localization accuracy cover estimations on the $X-Y$ plane as well as the Z-axis. These calculations are applied to every location within the domain $\mathbb{T}$. The domain for receiver placement, marked as the set $\mathbb{R}$, includes the allowable area for situating the receivers of the passive radar system.

2) Placement Framework: To reduce computation time, we developed a program that employs the class of evolutionary algorithms (EAs).

At the start of our EA process, we create a collection of P_T random individuals. Each individual consists of five receivers, randomly selected from the domain $\mathbb{R}$. To avoid the potential of settling into local minima, we distribute these individuals across various groups.

After the initial population is generated, individuals are sorted according to their fitness (cost) function value, with the selection for reproduction depending on these outcomes. The fitness function, calculated as the average $G(x,y,z)$ across the entirety of set $\mathbb{T}$ for a given configuration of five receivers, acts as the selection criterion. Following this, the algorithm selects the top P_s individuals to serve as the parent group for generating new offspring.

In the parent group, every adjacent pair of individuals undergoes a crossover process, producing $P_s/2$ offspring in total. The fitness function for each new individual is reassessed by the algorithm. Out of the total population of $P_n = P_T + P_s/2$, the $P_k = P_s/2$ individuals with the lowest fitness are eliminated, leaving a population of P_T individuals for the next iteration.

During the creation of new offspring, each pair of parents has a combined total of eight receivers, with each parent contributing four. The crossover method employed swaps the coordinate parameters of the first set of four receivers with those from the second set.

After completing the predetermined number of iterations, N_{iter}, the algorithm selects the top-ranked individual according to the fitness function. If this individual's $\overline{G(x,y)}$ and $\overline{G(z)}$ are both beneath the threshold values h_T and v_T, respectively, it is deemed the optimal solution. This solution then defines the placement configuration for the five receivers.

If the chosen individual fails to satisfy the required criteria, the algorithm resets, creating a new set of P_T individuals and

Algorithm 1 Passive Radar Receiver Deployment Algorithm

Input: Target domain ($\mathbb{T}$), Receiver domain ($\mathbb{R}$), $\overline{G(x,y)}$ threshold (h_T), $\overline{G(z)}$ threshold (v_T)
Output: Placement of a set of five receivers

```
while G(z) > v_T & G(x,y) > h_T do
    Generate a set of P_T random individuals, where each individual is a set of five receiver anchors
    for i = 1 to i = number of iteration do
        Check the fitness of all available individuals;
        Kill the worst ones to keep having P_T individuals;
        Select the individuals with better fitness as parents;
        Crossover adjacent parents, make an offspring;
    end for
end while
```

Table III: Non-optimized arbitrary receiver placement for different dimensions and altitudes

Altitudes	RX #1	RX #2	RX #3	RX #4	RX #5
Low (10m to 100m)	(17,20,1)	(32,22,1)	(89,,70,1)	(18,21,0)	(91,71,1)
Medium (100m to 500m)	(81,379,2)	(175,343,1)	(265,416,1)	(168,150,1)	(211,180,1)
High (500m to 1km)	(744,106,2)	(463,212,0)	(824,175,1)	(666,894,2)	(703,154,2)

Table IV: Receiver placement for different dimensions and altitudes with CARTA optimal solution

Altitudes	RX #1	RX #2	RX #3	RX #4	RX #5
Low (10m to 100m)	(0,0,2)	(100,0,2)	(100,100,0)	(0,100,2)	(50,50,1)
Medium (100m to 500m)	(0,0,1)	(500,0,1)	(500,500,1)	(0,500,1)	(250,250,2)
High (500m to 1km)	(0,0,1)	(900,0,1)	(900,900,1)	(0,1000,1)	(500,500,2)

restarting the process. This cycle of iteration persists until a solution is found that adheres to the predefined constraints.

V. Performance Evaluation

In this section, our discussion is structured in two stages. First, we showcase the results obtained from random receiver placements, highlighting the significant impact of geometric factors on the GDOP and overall positioning accuracy. Following this initial analysis, we delve into a detailed evaluation of the outcomes derived from applying the *CARTA* optimal placement framework, which allows us to examine the effectiveness of our suggested algorithm.

The simulations were executed using *MATLAB 2022a* on a *Dell Optiplex 7080* system, focusing on the deployment of five Starlink receivers. These simulations leverage parameters from the High-Performance Starlink dish in our inventory, grounding our simulations in practical, real-world conditions and making future real-life applications feasible. The chief objective of these simulations is to ascertain the most effective layout for the receivers. This optimal layout is crucially influenced by the spatial configuration of the intended protective zone and the altitude range required for detection. To this end, *CARTA* utilizes the specified protection area and necessary detection altitude as inputs to determine the receivers' optimal placement. To that end, for evaluation of the algorithm's effectiveness and adaptability, it has been tested on three distinct scenarios, each representing different dimensions and altitudes. *CARTA* is expected to perform particularly well in environments with more compact dimensions and reduced altitudes. Remarkably, it has proven its ability to generate optimal configurations effectively, even within considerably vast areas and across extensive altitude ranges.

The comparisons between non-optimized benchmarks and the *CARTA* optimized placements are detailed in Table III for the former and Table IV for the latter. All values are provided in meters for consistency and ease of comparison.

Our aim is to depict the xDOP metrics, which include HDOP, VDOP, and GDOP, designated as $G(.)$ values, specifically $G(x, y)$, $G(z)$, and $G(x, y, z)$, across 3D spaces. By calculating the mean xDOP values for every (x, y) location over all z levels, we intend to display these averages using heatmaps. This method not only simplifies the visualization of spatial data but also ensures a thorough consideration of all z levels, rather than focusing on a select few, thereby yielding a more comprehensive analysis.

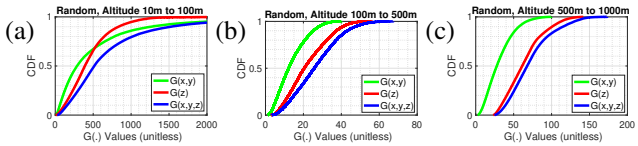

Figure 6: CDF plot representation of $G(.)$ values for various altitudes with random configuration from Table III

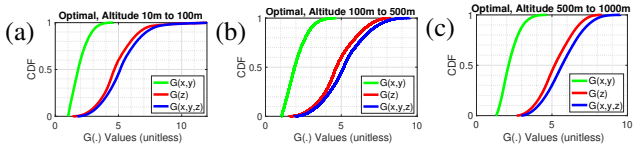

Figure 7: CDF plot representation of $G(.)$ values for various altitudes with optimal configuration shown in Table IV

To differentiate the specific effects on localization precision between the $X - Y$ plane and the Z-axis, we present HDOP and VDOP separately. This allows us to emphasize situations where a given arrangement might result in favorable horizontal accuracy but less desirable vertical estimations, thereby offering a more detailed understanding of performance nuances.

Figure 5 presents a comparative evaluation of xDOP values, encompassing both arbitrary and *CARTA* optimized placements. All the xDOP values are unitless numbers that scale the variance of distance measurements, directly impacting the final localization accuracy. Hence, lower values are preferable. Specifically, values below 5 are considered very good, between 5 and 10 good, 10 to 15 medium, 15 to 20 sufficient, and any value above 20 is deemed bad, as shown in Table II. This grading is visually represented in the figure through a heatmap, transitioning from blue (indicating lower values) to red (indicating higher values). The depicted outcomes consistently indicate favorable results across all examined scenarios, affirming the effectiveness of the *CARTA* algorithm.

Furthermore, the figure emphasizes the importance of utilizing the proposed optimization algorithm for receiver deployment over a random placement approach. This preference is supported by the significant impact of GDOP values on the overall accuracy of the system's precise localization capability, whether employing forwardscatter or backscatter. To mitigate the multiplicative effect in the equation $\sigma_T^2(x, y, z) = G(x, y, z) \cdot \sigma_r^2$, it is imperative to attain lower GDOP values. By introducing the *CARTA* optimal placement framework, we have successfully achieved this objective.

In Figure 7, the cumulative distribution function (CDF) of $G(.)$ values for optimal placement across three setups is illustrated. This analysis is intended to demonstrate the distribution of points in set $\mathbb{T}$ with $G(x, y, z)$ values below a certain threshold. The optimization goal was to ensure that the

majority of points had $G(x, y, z)$ values below 20, a target that has been successfully attained across all scenarios, as depicted in the figure.

To set a benchmark and underscore the significance of optimal placement, we present in Figure 6 analogous plots to those in Figure 7, but with random placement. As depicted in this figure, the $G(x, y, z)$ values soar to several hundreds, rather than predominantly remaining below 20. This indicates that without the *CARTA* optimal placement strategy, the accuracy of 3D localization may be unreliable owing to the elevated $G(x, y, z)$ values.

VI. Conclusion & Future Work

Conclusion: In this paper, we introduce *CARTA*, an approach that focuses on the optimal deployment of receivers for passive radar systems. Although *CARTA* is suitable for any passive system using any type of illuminators, we specifically concentrate on spaceborne illuminators, with an emphasis on the Starlink in the LEO constellation. This choice is due to their extensive coverage and their capability to detect low-observable targets. We derived the PEB for TDOA-based trilateration system used in *CARTA* and attributed the overall errors to ranging and geometry-related errors. *CARTA* proposes an optimization framework based on the EA class solutions to address the NP-Hard problem of finding the optimal deployment of receivers. Our results indicate that using *CARTA* can achieve a better overall GDOP compared to other arbitrary placements. This implies that the final 3D error of the target localization can achieve significantly better accuracy.

Future Work: Currently, we are advancing our experimental setup in real-life scenarios using the High-Performance model of Starlink receivers, which are suitable for mobile scenarios. The primary goal is to deploy the satellite receivers at locations identified by *CARTA* and evaluate the accuracy of target localization by comparing the proposed locations to a known ground truth location. To this end, preliminary tests have already been conducted, utilizing our Starlink dish to measure one-way latency time across various locations. Our ongoing effort is to establish a comprehensive passive detection setup with optimally placed Starlink receivers.

References

[1] "UAS sightings report," https://www.faa.gov/uas/resources/public_records/uas_sightings_report/, accessed: 2021-10-07.

[2] A. Famili, A. Stavrou, H. Wang, P. Jung-Min, and R. Gerdes, "Securing your airspace: Detection of drones trespassing protected areas," 2021. [Online]. Available: https://arxiv.org/abs/2111.03760

[3] D. Qi, F. Boyu, W. Feng, Z. Zhang, X. He, and C. Shang, "Digital TV signal based airborne passive radar clutter suppression via a parameter-searched algorithm," *Wireless Personal Communications*, vol. 120, pp. 1–28, 10 2021.

[4] M. Malanowski and K. Kulpa, "Two methods for target localization in multistatic passive radar," *IEEE Transactions on Aerospace and Electronic Systems*, vol. 48, pp. 572–580, 2012.

[5] A. Famili and J.-M. J. Park, "ROLATIN: robust localization and tracking for indoor navigation of drones," in *2020 IEEE Wireless Communications and Networking Conference (WCNC) (IEEE WCNC 2020)*, 2020.

[6] J. V.-V. Gerwen, K. Geebelen, J. Wan, W. Joseph, J. Hoebeke, and E. De Poorter, "Indoor drone positioning: Accuracy and cost trade-off for sensor fusion," *IEEE Transactions on Vehicular Technology*, vol. 71, no. 1, pp. 961–974, 2022.

[7] G. Chi, Z. Yang, J. Xu, C. Wu, J. Zhang, J. Liang, and Y. Liu, "Wi-Drone: Wi-Fi-based 6-DoF tracking for indoor drone flight control," in *Proceedings of the 20th Annual International Conference on Mobile Systems, Applications and Services*, ser. MobiSys '22. New York, NY, USA: Association for Computing Machinery, 2022, p. 56–68. [Online]. Available: https://doi.org/10.1145/3498361.3538936

[8] A. Famili, A. Stavrou, H. Wang, and J.-M. J. Park, "PILOT: high-precision indoor localization for autonomous drones," *IEEE Transactions on Vehicular Technology*, pp. 1–15, 2022.

[9] J. C. McDowell, "The low earth orbit satellite population and impacts of the SpaceX starlink constellation," *The Astrophysical Journal*, vol. 892, no. 2, p. L36, apr 2020. [Online]. Available: https://doi.org/10.3847/2041-8213/ab8016

[10] P. LACOMME, J.-P. HARDANGE, J.-C. MARCHAIS, and E. NORMANT, "Air and spaceborne radar systems," in *Air and Spaceborne Radar Systems*. Norwich, NY: William Andrew Publishing, 2007, pp. 1–504. [Online]. Available: https://www.sciencedirect.com/science/article/pii/B9781891121135500334

[11] J. Robie, A. Famili, and A. Stavrou, "Receiver density analysis for high probability detection of forward scattered airborne signals," in *2022 International Conference on Electrical, Computer and Energy Technologies (ICECET)*, 2022, pp. 1–6.

[12] B. Yonel, I.-Y. Son, and B. Yazici, "Exact multistatic interferometric imaging via generalized wirtinger flow," *IEEE Transactions on Computational Imaging*, vol. 6, p. 711–726, 2020. [Online]. Available: http://dx.doi.org/10.1109/TCI.2020.2967151

[13] M. Antoniou, Z. Zeng, L. Feifeng, and M. Cherniakov, "Experimental demonstration of passive bsar imaging using navigation satellites and a fixed receiver," *IEEE Geoscience and Remote Sensing Letters - IEEE GEOSCI REMOTE SENS LETT*, vol. 9, pp. 477–481, 05 2012.

[14] K. Gronowski, P. Samczyński, K. Stasiak, and K. Kulpa, "First results of air target detection using single channel passive radar utilizing GPS illumination," *2019 IEEE Radar Conference (RadarConf)*, pp. 1–6, 2019.

[15] V. Burov, A. Myakinkov, A. Ryndyk, R. Fadeev, D. Balashova, and A. Blyakhman, "Multi-static forward scatter radar with illumination from telecommunication satellites for detection of airborne targets," in *2018 19th International Radar Symposium (IRS)*, 2018, pp. 1–10.

[16] R. S. A. Raja Abdullah, S. Alhaji Musa, N. E. Abdul Rashid, A. Sali, A. A. Salah, and A. Ismail, "Passive forward-scattering radar using digital video broadcasting satellite signal for drone detection," *Remote Sensing*, vol. 12, no. 18, 2020. [Online]. Available: https://www.mdpi.com/2072-4292/12/18/3075

[17] H. Wang, N. Rajagopal, A. Rowe, B. Sinopoli, and J. Gao, "Efficient beacon placement algorithms for time-of-flight indoor localization," in *Proceedings of the 27th ACM SIGSPATIAL International Conference on Advances in Geographic Information Systems*, ser. SIGSPATIAL '19. New York, NY, USA: Association for Computing Machinery, 2019, p. 119–128. [Online]. Available: https://doi.org/10.1145/3347146.3359344

[18] R. Sharma and V. Badarla, "Analysis of a novel beacon placement strategy 3D localization in indoor spaces," in *11th International Conference on Communication Systems Networks (COMSNETS)*, Jan 2019, pp. 320–327.

[19] J. Schmalenstroeer and R. Haeb-Umbach, "Investigations into bluetooth low energy localization precision limits," in *2016 24th European Signal Processing Conference (EUSIPCO)*, Aug 2016, pp. 652–656.

[20] A. Famili, A. Stavrou, H. Wang, and J.-M. Park, "iDROP: Robust localization for indoor navigation of drones with optimized beacon placement," *IEEE Internet of Things Journal*, vol. 10, no. 16, pp. 14 226–14 238, 2023.

[21] N. Rajagopal, S. Chayapathy, B. Sinopoli, and A. Rowe, "Beacon placement for range-based indoor localization," in *2016 International Conference on Indoor Positioning and Indoor Navigation (IPIN)*, Oct 2016, pp. 1–8.

[22] W. Dai, Y. Shen, and M. Z. Win, "A computational geometry framework for efficient network localization," *IEEE Transactions on Information Theory*, vol. 64, no. 2, pp. 1317–1339, 2018.

[23] T. Wang, Y. Shen, A. Conti, and M. Z. Win, "Network navigation with scheduling: Error evolution," *IEEE Transactions on Information Theory*, vol. 63, no. 11, pp. 7509–7534, 2017.

[24] J. Robie, A. Famili, and A. Stavrou, "Revisiting the spaceborne illuminators of opportunity for airborne object tracking," *Computer*, vol. 56, no. 1, pp. 82–92, 2023.